Received April 4, 2020, accepted April 15, 2020, date of publication April 20, 2020, date of current version May 4, 2020.

Digital Object Identifier 10.1109/ACCESS.2020.2988714

A Recognition System for Partially Occluded Dorsal Hand Vein Using Improved Biometric Graph Matching

FU LIU, SHOUKUN JIANG, BING KANG, AND TAO HOU

College of Communication Engineering, Jilin University, Changchun 130012, China

Corresponding author: Tao Hou (ht_happy@jlu.edu.cn)

This work was supported in part by the National Natural Science Foundation of China under Grant 51835006.

ABSTRACT Some portions of dorsal hand may be occluded due to injuries, pigmentation, or tattoos, which significantly affects the performance of dorsal hand vein recognition systems. Biometric graph matching is a common shape-based feature extraction algorithm for vein recognition. However, this method does not consider edge attributes, which can provide additional discrimination ability. We present an improved biometric graph matching method that includes edge attributes for graph registration and a matching module to extract discriminating features. Moreover, we propose a recognition system for partially occluded dorsal hand vein. A database of normal hand vein images, three databases of images with artificially occluded dorsal hand vein with occlusions in different positions and ratios, and a database of images with tattooed hands are established to verify the validity of the proposed method. The experimental results demonstrated that the equal error rates and the accuracies were 0.0202 and 98.09% $\pm$ 0.28%, respectively for the normal hand vein images, 0.0453 and 96.58% $\pm$ 0.34%, respectively for images of artificially occluded dorsal hand vein with occlusion at all positions and area ratios ($0-20\%$, mean occluded area ratio = 9.3%), and 0.0343 and 97.14% $\pm$ 0.29%, respectively for the images of tattooed hands.

INDEX TERMS Dorsal hand vein recognition, biometric graph matching, occlusion, databases.

I. INTRODUCTION

Vein patterns in the dorsal hand are commonly used for biometric recognition and are detected using infrared light from the live body. Compared with other hand-based biometrics, such as fingerprints and palm print, the primary advantages of dorsal vein pattern identification are that no contact is required during image acquisition [1], and it is difficult to falsify the vein pattern [2]. Dorsal hand vein images are more conducive to collect vein pattern than palm, because the anterior surface of the palm is much thicker than the dorsal surface [3]. Thus, dorsal hand vein recognition has attracted broad interest in the field of biometric recognition.

Nowadays, many dorsal hand vein acquisition systems and feature description algorithms have been developed and were successfully used for dorsal hand vein recognition. For capturing vein patterns, the acquisition systems consist of 3 types of imaging approaches, including near infrared [4]–[6], far infrared [7], and hyperspectral techniques [8], [9].

The feature descriptors can be extracted using two types of algorithms: texture-based feature extraction algorithms and shape-based feature extraction algorithms [10], [11]. The former takes advantage of texture variations, and the statistical features of the texture are used for identification. For instance, Li and Kang introduced several improved variants of local binary patterns (LBP) to describe the characteristics of vein patterns [12]–[14]. Premalatha and Kumar investigated local phase quantization (LPQ) and its variants to develop a descriptor for individual identification [15], [16]. Wei extracted discriminative local features using hyperspectral images of dorsal hand vein [8]. Wang improved the scale-invariant feature transform (SIFT) method for use in cross-device hand vein recognition [17]. Meng and Wang used the Gabor filter and its variants to increase the discriminative power of feature descriptors and minimize the effects of noise, rotation, and shift [18], [19]. Generally, texture-based feature extraction algorithms focus on texture

The associate editor coordinating the review of this manuscript and approving it for publication was Alberto Cano.

variations, but do not consider the holistic geometric shape of vein pattern, thus leaving room for improving the recognition accuracy [11]. More importantly, texture-based features are not the essential distinction between individuals and are not robust to changes in lighting conditions [10].

Unlike texture-based feature extraction algorithms, shape-based feature extraction algorithms are robust to different lighting conditions and consider holistic geometric shape of vein pattern, which is unique in each person [11]. Typically, these algorithms segment the vein area and subsequently abstract the skeletons and extract the shape features. For example, many studies have extracted important points, such as endpoints [20], crossing points [6], [21] and vein minutiae [22]–[26], to describe their distinctiveness. However, few studies considered the holistic shape attributes, which are crucial for identification. Huang *et al.* proposed a spatial graph method that considered the minutiae of the vein skeleton and used factorized graph matching (FGM) to capture the shape attributes [11]. Biometric graph matching (BGM) was proposed by Lajevardi to improve the system's robustness to translation, nonlinear distortion, and small rotation [27], [28]. The BGM algorithm used the vein skeleton to generate a spatial graph and found the maximum common subgraph (MCS) between two graphs. The topological measures of MCS were used to determine whether the individual is a genuine. It is noteworthy that BGM is a modular approach, and additional features, such as vein length and vein width, can be added as attributes of the graph to increase the distinctiveness [29]. Zhong used BGM to create a dorsal hand vein recognition system for uncontrolled environments [30], [31]. Although the BGM algorithm has been used successfully for hand vein authentication, it does not consider the vascular connections (i.e., the edge attributes of graph), which are important aspects of the vein pattern.

Therefore, we present an improved BGM (IBGM) method for dorsal hand vein recognition systems. The IBGM makes better use of the edge attributes of the vein pattern than the BGM for extracting discriminating features. Using optimization, the IBGM eliminates repetitive computation of edge/vertex matching in the graph matching module, thereby improving the efficiency of the method. A recognition system for partially occluded dorsal hand vein is established to verify the validity of the IBGM. Experiments are performed on images of normal (non-occluded) hand vein, artificially occluded hand vein, and tattooed hand vein.

The remainder of the paper is organized as follows. Section 2 provides an overview of the BGM, and the IBGM approach is described in section 3. Section 4 introduces the recognition system, the image databases, and the performance evaluation approaches. The experimental results are provided in section 5. Section 6 concludes the paper and provides perspectives for future studies.

II. OVERVIEW OF BGM

The BGM takes into account the geometric shape of the vein, which is an essential factor in determining differences between individuals. Thus, the BGM has been used successfully for hand vein authentication under controlled and uncontrolled conditions [28] - [30], [32]. Generally, the BGM algorithm consists of three parts, including graph registration, graph matching and measurement of distance features.

A. GRAPH REGISTRATION

In this phase, the graphs are registered using only the vertices. For each edge pair whose edges belong to different graphs, the similarity based on the length and slope attributes is defined. Based on the similarity, the top N edge pairs are used to find the best registration. Each chosen edge pair is treated as the origin and positive x-axis of a Cartesian coordinate system, and the remaining vertices are transformed accordingly [29]. Subsequently, the number of corresponded vertices between the two graphs is counted. As defined in (1), a pair of vertices correspond if the Euclidean distance between their coordinates is below a threshold, the number of corresponded vertices, V_k, is increased by one and the vertices are labeled registered.

$$V_k = \begin{cases} V_k + 1 & if \ \sqrt{\left(x_{g_1} - x_{g_2}\right)^2 + \left(y_{g_1} - y_{g_2}\right)^2} < \varepsilon \\ V_k & else \end{cases}. \quad (1)$$

where V_k is the number of corresponded vertices when the kth pair of edges are located on positive x-axis ($k = 1, 2, \cdots, N$). $\left(x_{g_1}, y_{g_1}\right)$ and $\left(x_{g_2}, y_{g_2}\right)$ represent the unlabeled vertices from graph g_1 and g_2 respectively, and ε is a threshold.

The distance score, d_k, which represents the similarity between the graphs when the kth pair of edges are the origin and positive x-axis, is defined in (2). When d_k reaches the minimum, the best aligned graphs g_{out} and g'_{out} are obtained and are used as the input of graph matching.

$$d_k = 1 - \frac{V_k}{\sqrt{m_1 \times m_2}}. \quad (2)$$

where d_k is a distance score; m_1 and m_2 represent the numbers of vertices in graph g_1 and g_2, respectively.

B. GRAPH MATCHING

Subsequently, graph matching is used to extract the MCS, whose topological attributes are used to distinguish between an impostor and a genuine. A clever modification of Hungary's algorithm is proposed to extract the MCS. As defined in [33], the cost matrix represents the edit cost to convert g_{out} to g'_{out}.

$$\boldsymbol{C}_{cost} = \begin{bmatrix} \boldsymbol{C} & \boldsymbol{D} \\ \boldsymbol{S} & \boldsymbol{0} \end{bmatrix}. \quad (3)$$

where $\boldsymbol{C} = \left[c_{ij} | 1 \le i \le m_1, 1 \le j \le m_2\right]$ and c_{ij} represents the cost of substituting vertex between g_{out} and g'_{out}. The diagonal elements, d_{ii} of $\boldsymbol{D}$ and s_{jj} of $\boldsymbol{S}$ indicate the cost of deleting points in g_{out} and the cost of inserting points in g'_{out}. All elements outside the main diagonal of $\boldsymbol{D}$ and $\boldsymbol{S}$ are equal

to ∞ [34].

$$c_{ij} = \sqrt{\left(x_i - x'_j\right)^2 + \left(y_i - y'_j\right)^2}. \quad (4)$$

$$d_{ii} = 5 \times (1 + De(v_i)). \quad (5)$$

$$s_{jj} = 5 \times \left(1 + De\left(v'_j\right)\right). \quad (6)$$

where v_i and v'_j are the ith vertex of g_{out} and the jth vertex of g'_{out}; the corresponding coordinates are (x_i, y_i) and $\left(x'_j, y'_j\right)$, and $De(\bullet)$ is a degree (number of incident edges).

C. MEASUREMENT OF DISTANCE FEATURES

Finally, four distance features based on the MCS's topological characteristics are used to determine whether the individual is a genuine [29].

i. The distance based on the vertices, d_v, is defined in (7):

$$d_v = 1 - \frac{\left|MCS\left(g_{out}, g'_{out}\right)\right|_v}{\sqrt{|g_{out}|_v \left|g'_{out}\right|_v}}. \quad (7)$$

where $|\bullet|_v$ represents the number of vertices in the spatial graph.

$C2$ represents the number of vertices in the two largest connected components in the MCS;

δ_d^2 represents the variance of the vertex degree distribution of the MCS;

ii. The distance based on the edges, d_e, is defined in (8).

$$d_e = 1 - \frac{\left|MCS\left(g_{out}, g'_{out}\right)\right|_e}{\sqrt{|g_{out}|_e \left|g'_{out}\right|_e}}. \quad (8)$$

where $|\bullet|_e$ represents the number of edges in the spatial graph.

III. IMPROVED BIOMETRIC GRAPH MATCHING

The BGM only uses the attributes of the vertices [34] but does not consider the edge attributes; thus there is room for improving the accuracy. Moreover, the edge attributes are also crucial for the identification of individuals. Therefore, we propose the IBGM to extract more discriminating features by including edge attributes in the graph registration and matching. The modified algorithm IBGM is described as follows:

A. MODIFIED GRAPH REGISTRATION

In this phase, the graphs are registered using the vertices and the edges. A pair of vertices correspond is defined in (1); similarly, we define a pair of edges correspond as (9). The corresponded edges are labeled registered.

$$E_k = \begin{cases} E_k + 1 & if \begin{pmatrix} \dfrac{abs\left(l_{g_1} - l_{g_2}\right)}{\max\left(l_{g_1}, l_{g_2}\right)} \le \varepsilon_l \\ \&abs\left(\theta_{g_1} - \theta_{g_2}\right) < \varepsilon_\theta \end{pmatrix} \\ E_k & else \end{cases}. \quad (9)$$

where E_k is the number of corresponded edges when the kth pair of edges are located on positive x-axis. l_{g_1}, l_{g_2} and θ_{g_1}, θ_{g_2} represent the lengths and angles of the unlabeled edges in graph g_1 and g_2. In this study, the values are chosen empirically and are ε_l= 20% and ε_θ=22.5°.

Based on the premise that edges have more information than vertices, the distance score which is defined in (2), is redefined as (10). The attributes of the edges are added to the distance score and receive higher weights than those of the vertices. When d_k reaches the minimum, we obtain the best aligned graphs g_{out} and g'_{out}.

$$d_k = \left(1 - \frac{E_k}{\sqrt{n_1 \times n_2}}\right) + w\left(1 - \frac{V_k}{\sqrt{m_1 \times m_2}}\right). \quad (10)$$

where d_k is a new distance score. E_k and V_k are the number of corresponded edges and vertices, n_1, n_2 and m_1, m_2 are the number of edges and vertices in graph g_1 and g_2, respectively. In this study, w is equal to 0.1.

B. MODIFIED GRAPH MATCHING

In this study, we use both edge and vertex attributes to find the MCS. According to the modified graph registration module, several matched edges (for instance, the edge pair located on positive x-axis) and the corresponded vertices do not need to match repeatedly in graph matching. Thus, we modify the graph matching module to reduce the computational complexity. The details are as follows:

First, the matched edges and corresponded vertices (called V_e) in the registration module are labeled and do not need to match repeatedly.

Second, we match the unmatched vertices using a modification of Hungary's algorithm (called V_m). Accordingly, the size of the cost matrix $\boldsymbol{C}_{cost}$ changes from $(m_1 + m_2) \times (m_1 + m_2)$ to $(m_1 + m_2 - 2p) \times (m_1 + m_2 - 2p)$, where m_1 and m_2 are the numbers of vertices in g_{out} and g'_{out}, and p is the size of V_e. This approach improves the point matching efficiency due to the smaller size of $\boldsymbol{C}_{cost}$.

Finally, we match the unmatched edges whose vertices are either obtained from V_e and V_m or from V_m. The improved MCS is defined by the matched vertices and edges.

C. MODIFIED MEASUREMENT OF DISTANCE FEATURES

Six distance features are used to describe the topological attributes; the four features d_v, $C2$, δ_d^2, and d_e are the same as in Section 2, and two new features are included. The new distance score based on the edges, s_e, is defined in (11) and (12).

$$s_e = \sum_{i=1}^{n_m - 1} f_i(v). \quad (11)$$

$$f(v) = \omega_1 \times num_m + \omega_2 \times num_e. \quad (12)$$

where n_m is the number of matched edge pairs. The edge that is located on x-axis is not considered in this score. $f(v)$ is the score of an edge pair, which is defined empirically in (12). Different weights (ω_1 and ω_2) are used to increase the discrimination ability. num_m represents the number of

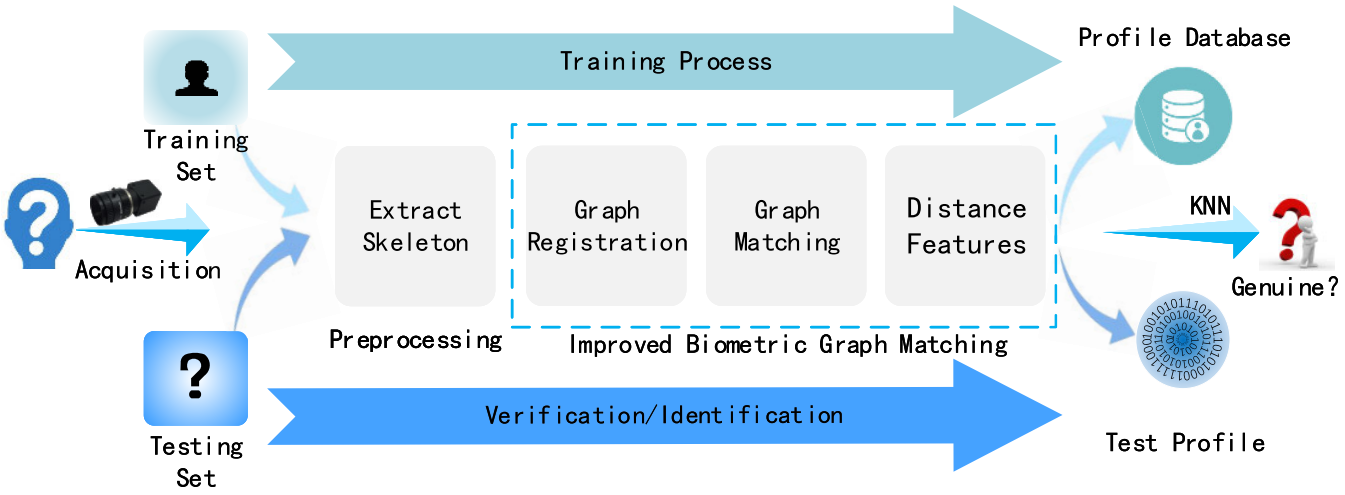

FIGURE 1. The flowchart of the recognition system.

vertices obtained from V_m and num_e represents the number of vertices obtained from V_e. In this study, the values of ω_1 and ω_2 are 0.1 and 0.25, respectively. There are four vertices in a matched edge pair. If three vertices are from V_m and one vertex is from V_e, the score $f(v)$ is 0.55.

The second new distance feature, the overlap area ratio, k_r, is defined in (13). k_r from a genuine person is typically larger than that from an impostor.

$$k_r = \frac{overlap\ area}{ROI\ area}. \tag{13}$$

where the overlap area is the intersection of two images after the MCS has been obtained. The region of interest (ROI) is 256X256 pixels in this study.

IV. DORSAL HAND VEIN RECOGNITION SYSTEM

Dorsal hand vein may be occluded due to injury or pigmentation, which may lower the performance of the recognition system. Therefore, it is crucial to be able to extract discriminating features from occluded hand vein. We propose a recognition system for partially occluded dorsal hand vein using IBGM, which is capable of extracting more discriminating features than BGM.

Fig.1 illustrates the flowchart of the recognition system. First, the acquisition system is used to collect dorsal hand vein images to establish the training set and testing set. Subsequently, the sets are used during the training process and verification/identification process. During the training stage, the training set is used for skeleton abstraction and feature extraction. The IBGM is used to obtain the distance features to construct a profile database. Following the same procedures, a test profile is created during the verification/identification stage. Finally, the k-nearest neighbor (KNN) is used to compare the profile database with the test profile to determine if the test person is an authorized user (verification) or to identify who the test person is (identification).

A. THE ACQUISITION SYSTEM

The vein structure beneath the skin cannot be detected using visible light. However, near-infrared (NIR) light penetrates deeper into biological tissues and is used as a light source to capture hand vein images. We designed an image acquisition system to collect one spectral dorsal hand vein images. Fig.2a shows the system that consists of six components: 1) a protective box, 2) a low-cost NIR CMOS camera, 3) an optical lens, 4) an NIR light source, 5) a light diffuser, and 6) a hand grip. The NIR LEDs are evenly and circumferentially located around the camera to collect high-quality vein images. In this work, a light diffuser is used to produce parallel light rays to avoid bright spots in the vein images. The NIR light in natural light is blocked by the protective box to avoid light effects in the images. The hand grip is used to constrain the volunteer's hand and to be able to change the posture. The most important part of the acquisition system is the NIR CMOS camera, which is used to collect the dorsal hand vein images; the spatial resolution of the camera is 320X240 pixels. Examples of vein images are shown in Fig.2b.

B. HAND VEIN DATABASES

In this study, five databases of dorsal hand vein images were created, including a database of normal hand vein (NHV), three databases with artificially occluded vein (AOV_1 - AOV_3), and a database with tattooed hand vein (THV), to verify the performance of the IBGM. Compared with other published hand vein datasets, we collected vein images that were occluded due to injuries, pigmentation, or tattoos. The images in the databases were obtained using the acquisition system shown in Fig.2a. The NHV contains 3680 ROIs (ROI extraction is described in the next section) of normal right-hand vein images from 736 individuals, with

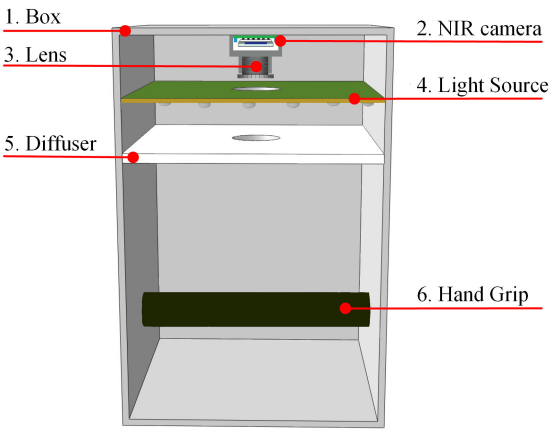

(a) Acquisition system

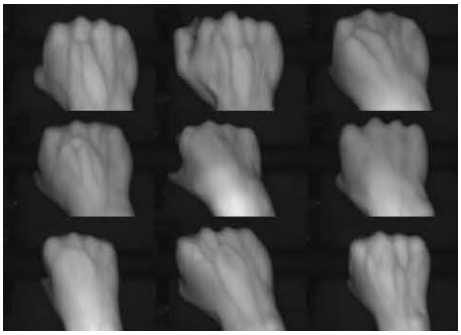

(b) Raw dorsal hand vein images

FIGURE 2. **The proposed acquisition system and captured vein images. (a) The image acquisition system consists of the (1) protective box, (2) NIR camera, (3) optical lens, (4) light source, (5) diffuser, and (6) hand grip. (b) Raw dorsal hand vein images obtained with our acquisition system.**

five samples per person (the raw dorsal hand vein images are freely available at https://github.com/JLUqiankun/Vein). The ROIs in the NHV are shown in Fig.3a. The AOV_1 - AOV_3 contains artificially occluded vein images from the NHV; the same 50% of the images (called test ROIs) from the NHV are occluded with different positions and levels of occlusion. Fig.3b - 3d show examples of the AOV_1, AOV_2, and AOV_3, respectively. In AOV_1, the test ROIs are artificially occluded at different positions with different area ratios (5%, 10%, 15%, and 20%). In AOV_2, the test ROIs are artificially occluded at different positions (nine positions) with the same occluded area ratio (10%). Fig.3e shows an example of a vein pattern that is divided into $3 * 3$ blocks and is used in the AOV_2. In AOV_3, the test ROIs are artificially occluded at different positions with different area ratios ($0 - 20\%$, mean occluded area ratio $= 9.3\%$) because the location and area of tattoos are random on people's hands. The THV consists of 250 normal dorsal hand vein images and tattooed dorsal hand vein images from 50 volunteers. The volunteers were asked to attach tattoo stickers to the back of their hands. Fig.3f illustrates typical examples of tattooed vein images. Additionally, as is common, most of the tattoos are located in the central area of the dorsal hand.

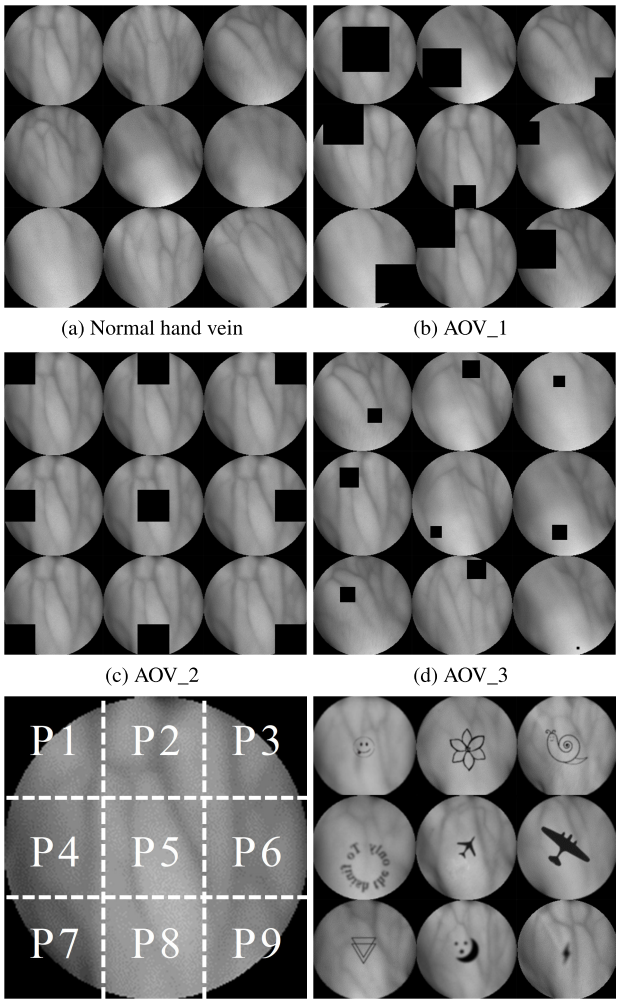

(a) Normal hand vein (b) AOV_1

(c) AOV_2 (d) AOV_3

(e) Subgraphs of ROI (f) Tattooed hand vein

FIGURE 3. **Typical samples of dorsal hand vein from (a) Normal hand vein. (b) AOV_1 occluded at different positions with different area ratios (5%, 10%, 15%, and 20%). (c) AOV_2 occluded at nine positions with the same occluded area ratio (10%). (d) AOV_3 occluded at different positions with different area ratios ($0 - 20\%$, mean occluded area ratio = 9.3%). (e) Normal vein image separated into $3 * 3$ blocks. (f) Tattooed hand vein images collected from hands with tattoo stickers.**

C. PREPROCESSING

Image preprocessing is a vital step in the recognition system to obtain vein graphs [30]. Fig. 4 illustrates the process of image preprocessing. First, we extract the boundary from raw dorsal hand vein image (Fig. 4(a)) by conditional random field [36], and a maximum inscribed circle based on Voronoi diagram [6] is adopted to locate the largest circular region as ROI; circular ROIs are preferred because of their larger area and entropy [37], [38]. Fig. 4(b) illustrates the maximum inscribed circle within the boundary of hand. Second, according to the location of circle in Fig. 4(b), we locate circular ROI on the hand (Fig. 4(c)) and extract circle ROI (Fig. 4(d)). The ROIs are normalized to 256X256 in the study. Finally, we use multi-matched filters as described in [28], to abstract the vein skeleton (Fig. 4(e)). The skeleton is abstracted by removing pixels at the boundaries and maintaining the connection between pixels using morphological operators [20].

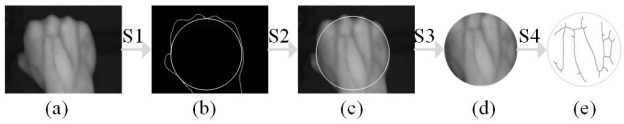

FIGURE 4. The process of image preprocessing. (a) Raw dorsal hand vein image. (b) The boundary of the hand and the maximum inscribed circle within the boundary. (c) The maximum inscribed circle with the boundary of hand. (d) Circular ROI. (e) Vein skeleton. (S1: Determining the boundary of the hand and locating the maximum inscribed circle. S2: The maximum inscribed circle on the hand. S3: Extraction of circular ROI. S4: Abstraction of the skeleton.).

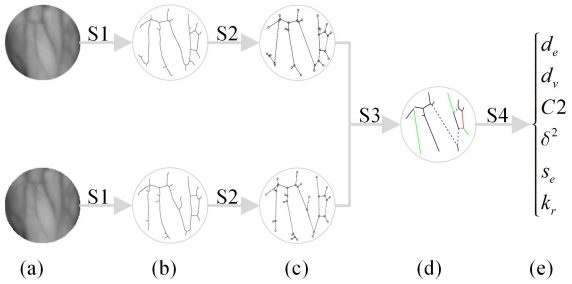

FIGURE 5. The process of the proposed IBGM. (a) Vein images. (b) Skeletons. (c) Spatial graphs. The circles and lines represent the vertices and edges respectively. (d) MCS. The red and black lines are the matched edges obtained from the graph registration module. The red line represents the x-axis during graph registration and matching. The vertices of the blue dotted lines are obtained from the black or red lines. Additionally, the vertices of the green lines are matched by the modification of Hungary's algorithm or one vertex is obtained from black or red lines. (e) Distance features. (S1: Abstraction of the skeleton. S2: Extraction of spatial graph. S3: Extraction of MCS. S4: Extraction of distance features.).

The edge with an endpoint is removed if its length is less than 20 pixels.

D. THE IBGM PROCESS

Fig.5 illustrates the process of the proposed IBGM. The vein images (Fig.5(a)) are used to abstract skeleton (Fig.5(b)) with multi-matched filters. Subsequently, we extract the vertices and edges (circles and lines in Fig.5(c), respectively). The key result (MCS) is shown in Fig.5(d). In Fig. 5(d), the red and black lines are the matched edges obtained from the graph registration module. The red line represents the x-axis during graph registration and matching. The vertices of the blue dotted lines are obtained from the black or red lines. Additionally, the vertices of the green lines are matched by the modification of Hungary's algorithm or one vertex is obtained from black or red lines. Finally, six distance features based on the MCS's topological characteristics are measured to determine whether the individual is a genuine (Fig.5(e)).

E. PERFORMANCE EVALUATION APPROACH

The performance of the IBGM is evaluated by determining the mean accuracy (ACC_{mean}), standard deviation of the accuracy (ACC_{std}), mean equal error rate (EER_{mean}), and runtime (RT) [37]. Additionally, the detection error trade-off (DET) curve is also used to assess the performance of the recognition system. The ACC_{mean} (14) and ACC_{std} (16) are used to evaluate the IBGM's accuracy and robustness using 100 times cross-validation. The higher the ACC_{mean}, the better the performance of the system is, the lower the ACC_{std}, the more robust the system is.

$$ACC_{mean} = \frac{\sum_{i=1}^{100} ACC_i}{100}. \tag{14}$$

where ACC_i is the recognition accuracy in the ith experiment, which is defined in (15).

$$ACC_i = \frac{Number\ of\ recognized\ images}{Number\ of\ test\ images} \times 100\%. \tag{15}$$

$$ACC_{std} = \sqrt{\frac{\sum_{i=1}^{100} (ACC_i - ACC_{mean})^2}{100}}. \tag{16}$$

The RT (17) is used to measure the IBGM's computational complexity, which is important in a real-time system.

$$RT = \frac{Run\ time\ for\ all\ testing\ images}{Number\ of\ testing\ images}. \tag{17}$$

The EER_{mean} (18) represents the IBGM's equal error rate. The lower the EER_{mean}, the higher the accuracy of the system is.

$$EER_{mean} = \frac{\sum_{i=1}^{100} EER_i}{100}. \tag{18}$$

where EER_i is the equal error rate in the ith experiment.

V. EXPERIMENTAL RESULTS AND DISCUSSION

We conducted detailed comparisons with similar algorithms, such as LBP [12], LPQ [15], Gabor [19], SIFT [17], FGM [11], and BGM [29] to determine the performance of the IBGM. We also tested the IBGM only using only edge attributes in the graph registration (IB0, short for IBGM with $w = 0$ in Eq. (10)). We evaluated the performance of IBGM using the NHV, AOV_1 to AOV_3, and the THV. In this study, the samples in the NHV and AOV_1 to AOV_3 were used to compare 7360 genuine comparisons and 270480 impostor comparisons of the first sample of each hand [30]. The samples in the THV were used to compare 1250 genuine comparisons and 12250 impostor comparisons. Seventy percent of the impostor and genuine comparisons were used to train the parameters using the KNN (K=1), and the rest were used for testing. For each database, we conducted experiments using 100 times cross-validation.

A. PERFORMANCE EVALUATION FOR THE NHV

Fig.6 shows the comparison of the performances of the proposed IBGM and the other methods. As illustrated in Fig.6a, the accuracies of the LBP, LPQ, Gabor, SIFT, FGM, BGM, and IB0 (only using edge attributes in graph registration) are 97.89% ± 0.29%, 96.83% ± 0.54%, 96.35% ± 0.55%, 96.67%±0.51%, 95.87%±0.78%, 96.82%±0.51%

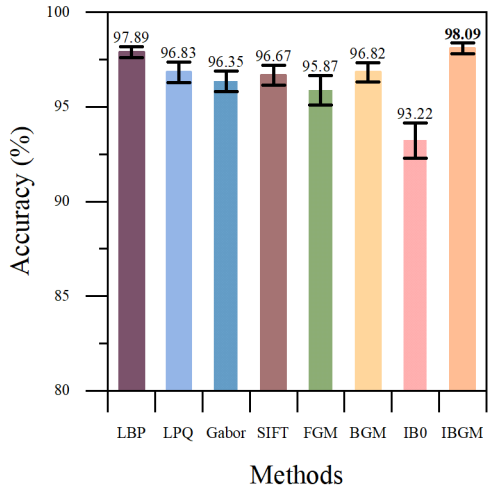

(a) Accuracy

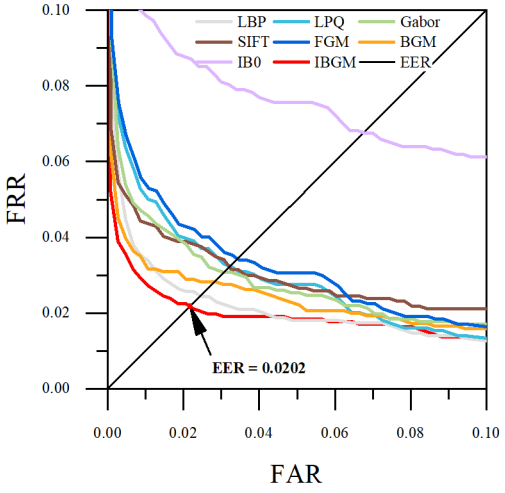

(b) DET curves

FIGURE 6. Comparative performance of IBGM and other methods (LBP, LPQ, Gabor, SIFT, FGM, BGM and IB0) on the NHV.

and 93.22% ± 0.93%. The LBP achieves the best performance among the seven typical methods in terms of accuracy, whereas the accuracy of the IBGM is 98.09% with a low standard deviation (0.28%). This result demonstrates that the IBGM achieves better recognition performance and robustness than the LBP. As shown in Fig.6b, the proposed IBGM has the lowest EER (0.0202, red dot in Fig.6b). The IBGM can extract more topology features than FGM and BGM, resulting in higher accuracy of recognition. The IB0, which uses only edge attributes for graph registration, has low distinctiveness of the features, adversely affecting its performance. Few SIFT feature points were extracted by the NHV, causing poor performance. The rotation and translation invariance of global features is better than that of local features; thus, the IBGM has better performance than LBP, LPQ, and Gabor. These results indicate that the IBGM outperforms all other methods in terms of accuracy, robustness, and EER.

TABLE 1. Comparative performance of IBGM and seven typical methods for the AOV_1 (occlusion at different positions with different area ratios (5%, 10%, 15%, and 20%)). Mean_5(10, 15, and 20), STD_5(10, 15, and 20), EER_5(10, 15, and 20) denote the mean, STD, and EER with 5% (10%, 15%, and 20%) occlusion, respectively.

Method	LBP	LPQ	Gabor	SIFT	FGM	BGM	IB0	IBGM
Mean_5(%)	91.97	92.33	93.38	96.69	94.03	95.47	91.53	97.51
STD_5(%)	0.48	0.43	0.39	0.21	0.30	0.29	0.57	0.14
EER_5(%)	8.28	8.17	7.18	3.92	6.56	5.03	9.89	3.23
Mean_10(%)	90.84	91.2	92.25	94.55	93.90	94.34	88.63	97.01
STD_10(%)	0.52	0.53	0.51	0.48	0.53	0.59	0.69	0.44
EER_10(%)	8.72	8.91	8.22	5.93	6.59	5.85	11.70	3.24
Mean_15(%)	88.08	88.43	90.46	93.65	90.08	91.48	86.09	94.45
STD_15(%)	0.58	0.56	0.63	0.53	0.70	0.82	0.76	0.47
EER_15(%)	11.07	11.95	10.87	7.29	10.18	10.51	14.04	6.53
Mean_20(%)	80.66	84.98	81.93	86.90	82.51	83.80	82.90	87.64
STD_20(%)	0.68	0.59	0.73	0.66	0.86	0.92	1.00	0.56
EER_20(%)	19.81	19.68	18.51	14.64	17.77	16.96	17.27	13.83

TABLE 2. Comparative performance of IBGM and seven typical methods for the AOV_2 (occlusion at 9 positions with the same occluded area ratio (10%)).

Methods	LBP	LPQ	Gabor	SIFT	FGM	BGM	IB0	IBGM
P1 (%)	91.90	91.84	92.78	96.25	93.51	94.94	89.09	97.26
P2 (%)	91.09	92.00	92.88	95.47	93.71	94.82	88.90	97.34
P3 (%)	91.05	91.38	92.00	95.54	93.33	94.63	90.01	96.80
P4 (%)	91.85	91.81	92.56	95.25	93.15	94.23	88.67	96.65
P5 (%)	90.89	91.70	92.94	95.74	93.01	94.57	89.98	96.46
P6 (%)	91.75	91.24	92.33	95.97	93.91	94.54	89.43	97.50
P7 (%)	92.26	92.01	94.54	96.80	94.79	95.66	88.69	97.64
P8 (%)	92.32	92.99	93.97	96.35	94.64	95.94	89.32	97.70
P9 (%)	92.30	92.89	93.37	96.80	94.72	95.97	89.75	97.78
Mean (%)	91.71	91.98	93.04	96.02	93.86	95.03	88.32	97.24
STD (%)	0.53	0.57	0.76	0.54	0.65	0.62	0.53	0.46
EER (%)	8.40	8.21	7.20	4.40	6.33	5.13	10.46	3.04

TABLE 3. Comparative performance of IBGM and seven typical methods for the AOV_3 (occlusion at different position with different area ratios (0 − 20%, mean occluded area ratio = 9.3%)).

Methods	LBP	LPQ	Gabor	SIFT	FGM	BGM	IB0	IBGM
Mean (%)	90.82	91.25	92.03	95.58	92.68	94.68	90.89	96.58
STD (%)	0.92	0.82	0.82	0.60	0.81	0.63	0.89	0.34
EER (%)	9.54	9.01	8.55	5.40	7.89	6.04	8.92	4.53

B. PERFORMANCE EVALUATION FOR THE AOVs

The performance results for the AOVs are shown in Table.1 - Table.3. Table.1 illustrates the recognition performance on the AOV_1. For every method, we observed that the larger the occluded area, the lower the accuracy is, and the larger the EER is. For instance, for 5%, 10%, 15%, and 20% occluded areas, the accuracies of SIFT are 96.69%±0.21%, 94.55%± 0.48%, 93.65%±0.53%, and 86.90%±0.66%, and the EERs are 3.92%, 5.93%, 7.29%, and 14.64%. The SIFT has the highest accuracy and lowest EER among the seven typical methods. As shown in Table.1, for different occluded areas, the IBGM has slightly higher accuracy and lower EER than SIFT. In summary, the proposed IBGM is robust to occlusion and has better performance than the other methods. As the area of occlusion increases, the accuracy decreases significantly.

The performance results for the AOV_2 are shown in Table.2. The LBP, LPQ, and Gabor have accuracies of

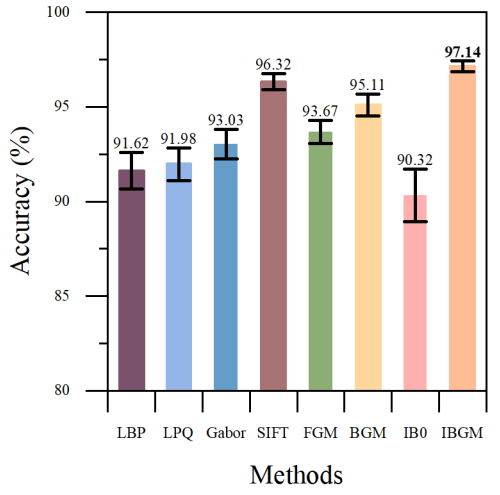

(a) Accuracy

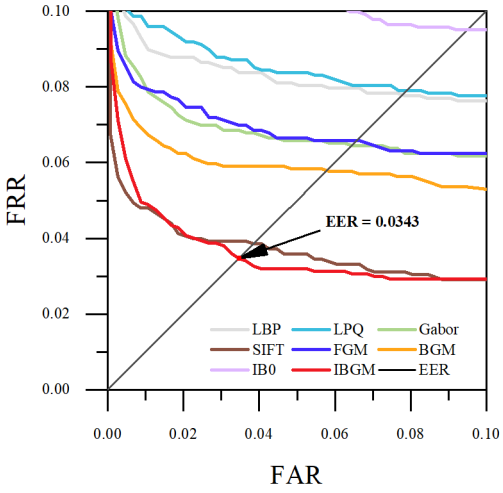

(b) DET curves

FIGURE 7. Comparative performance of IBGM and seven typical methods for the THV.

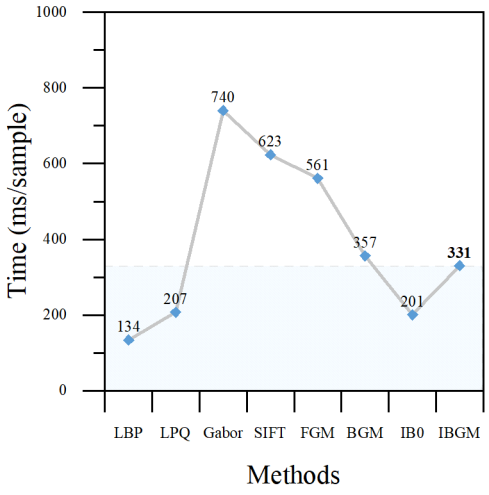

(a) Feature extraction time

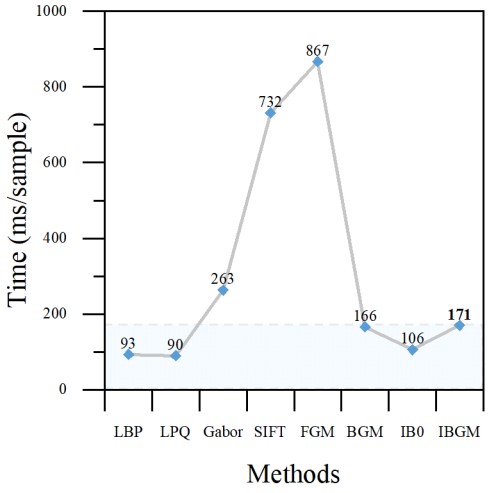

(b) Matching time

FIGURE 8. The computational complexity of the different methods.

91.71% ± 0.53%, 91.98% ± 0.57%, and 93.04% ± 0.76%; these three methods have the lowest accuracies. Thus, we can infer that the texture-based methods (LBP, LPQ, and Gabor) are sensitive to occlusion. The shape-based methods (FGM, BGM, and IBGM) have better recognition performance than the texture-based methods. Additionally, because the IB0 uses only edge attributes for graph registration, several registration failures occurred. Overall, the IBGM has the highest accuracy (97.24%±0.46%) and lowest EER (3.04%) for the AOV_2, which indicates its robustness to occlusion.

The performance results for the AOV_3 are shown in Table.3. The accuracies of the LBP, LPQ, Gabor, SIFT, FGM, BGM, and IB0 are 90.82% ± 0.92%, 91.25% ± 0.82%, 92.03%±0.82%, 95.58%±0.60%, 92.68%±0.81%, 94.68% ± 0.63%, and 90.89% ± 0.89%, respectively. The SIFT has the highest accuracy and robustness among the seven methods. The IBGM obtains the highest overall accuracy (96.58%) and the lowest standard deviation (0.34%). The shape-based methods (FGM, BGM, and IBGM) have higher performance than the texture-based methods (LBP, LPQ, and Gabor). It is likely that occlusion have a smaller impact on the shape than the texture.

C. PERFORMANCE EVALUATION FOR THE THV

The performance results for the THV are shown in Fig.(7). The accuracies of the LBP, LPQ, Gabor, SIFT, FGM, BGM, IB0, and IBGM are 91.62% ± 0.96%, 91.98% ± 0.86%, 93.03%±0.78%, 96.32%±0.42%, 93.67%±0.60%, 95.11% ± 0.57%, 90.32% ± 1.39% and 97.14% ± 0.29%. Because the texture features (LBP, LPQ, and Gabor) extracted from normal hand vein images and tattooed hand vein images exhibit large differences, the recognition performance is low

for the THV. Moreover, the tattooed stickers may occlude the no-vein area; thus, the global feature extraction algorithms (shape-based methods) are less affected by occlusion. As illustrated in Fig.(7), the shape-based methods (FGM, BGM, and IBGM) have higher accuracy than the texture-based methods (LBP, LPQ, and Gabor). The proposed IBGM has the lowest EER (0.0343, red dot in Fig.7b) and the highest accuracy, indicating that the IBGM is well suited for occluded vein recognition.

D. COMPUTATIONAL COMPLEXITY

The computational complexity of the different methods and the runtimes for the THV are shown in Fig.8. The algorithms are tested using MATLAB 2019a on a PC with Windows 10, Core i5 CPU (3.4 GHz), and 16G Ram. In terms of feature extraction time and matching time, the proposed IBGM (331 ms, 171 ms) is as fast as the BGM (357 ms, 166 ms) and faster than FGM (561 ms, 867 ms). The result demonstrates that eliminating repetitive computation of edge matching in the graph matching module improves the algorithm's efficiency even though the edge attributes are added. Moreover, Gabor (8 directions, 5 scales) is a multi-scale algorithm, and the number of features is high because not feature reduction was performed. SIFT has poor real-time performance. Thus, the feature extraction time and matching time of Gabor (740 ms, 263 ms) and SIFT (623 ms, 732 ms) methods are longer than those of the proposed IBGM. Only the LBP (134 ms, 93 ms), LPQ (207 ms, 90 ms), and IB0 (201ms, 106ms) are faster than the IBGM, but the proposed method provides better recognition performance (Fig.7). Overall, the extraction and matching times of the IBGM are acceptable.

VI. CONCLUSION AND FUTURE WORK

In this paper, we proposed the IBGM method by adding edge attributes to the graph registration and matching to improve the method's discriminative power in the presence of occlusion of dorsal hand veins. We established the NHV, AOVs, and THV, which were used to evaluate the performance of the proposed method. In comparison with seven other commonly used recognition methods, the IBGM provided the highest accuracy and the lowest EER for all databases. The extraction and matching times of the IBGM were acceptable. The results demonstrate the superior performance and robustness of the proposed IBGM.

In a future study, we will further improve the algorithm by focusing on two directions. (1) We will improve the recognition performance for the THV, and (2) we will collect more tattooed vein images and other occluded images to expand the database of occluded images.

REFERENCES

[1] Y. Wang, D. Zhang, and Q. Qi, "Liveness detection for dorsal hand vein recognition," *Pers. Ubiquitous Comput.*, vol. 20, no. 3, pp. 447–455, Jun. 2016.

[2] M. Z. Yildiz, O. F. Boyraz, E. Guleryuz, A. Akgul, and I. Hussain, "A novel encryption method for dorsal hand vein images on a microcomputer," *IEEE Access*, vol. 7, pp. 60850–60867, Mar. 2019.

[3] Gopal, S. Srivastava, S. Bhardwaj, and S. Bhargava, "Fusion of palm-phalanges print with palmprint and dorsal hand vein," *Appl. Soft Comput.*, vol. 47, pp. 12–20, Oct. 2016.

[4] W. Nie and B. Zhang, "Robust and adaptive ROI extraction for hyperspectral dorsal hand vein images," *IET Comput. Vis.*, vol. 13, no. 6, pp. 595–604, Sep. 2019.

[5] C.-L. Lin and K.-C. Fan, "Biometric verification using thermal images of palm-dorsa vein patterns," *IEEE Trans. Circuits Syst. Video Technol.*, vol. 14, no. 2, pp. 199–213, Feb. 2004.

[6] R. B. Trabelsi, A. D. Masmoudi, and D. S. Masmoudi, "A novel biometric system based hand vein recognition," *J. Test. Eval.*, vol. 42, no. 4, pp. 809–818, Jul. 2014.

[7] J. E. S. Pascual, J. Uriarte-Antonio, R. Sanchez-Reillo, and M. G. Lorenz, "Capturing hand or wrist vein images for biometric authentication using low-cost devices," in *Proc. 6th Int. Conf. Intell. Inf. Hiding Multimedia Signal Process.*, Darmstadt, Germany, Oct. 2010, pp. 318–322.

[8] W. Nie, B. Zhang, and S. Zhao, "Discriminative local feature for hyperspectral hand biometrics by adjusting image acutance," *Appl. Sci.*, vol. 9, no. 19, p. 4178, Oct. 2019.

[9] Y. Zhou and A. Kumar, "Human identification using palm-vein images," *IEEE Trans. Inf. Forensics Security*, vol. 6, no. 4, pp. 1259–1274, Dec. 2011.

[10] X. Li, D. Huang, R. Zhang, Y. Wang, and X. Xie, "Hand dorsal vein recognition by matching width skeleton models," in *Proc. IEEE Int. Conf. Image Process. (ICIP)*, Phoenix, AZ, USA, Sep. 2016, pp. 3146–3150.

[11] D. Huang, X. Zhu, Y. Wang, and D. Zhang, "Dorsal hand vein recognition via hierarchical combination of texture and shape clues," *Neurocomputing*, vol. 214, pp. 815–828, Nov. 2016.

[12] K. Li, G. Zhang, and Y. Wang, "Hand-dorsa vein recognition based on improved partition local binary patterns," in *Proc. CCBR*, Tianjin, China, 2015, pp. 312–320.

[13] W. Kang and Q. Wu, "Contactless palm vein recognition using a mutual foreground-based local binary pattern," *IEEE Trans. Inf. Forensics Security*, vol. 9, no. 11, pp. 1974–1985, Nov. 2014.

[14] Y. Wang, Q. Duan, L. K. Shark, and D. Huang, "Improving hand vein recognition by score weighted fusion of wavelet-domain multi-radius local binary patterns," *Int. J. Comput. Appl. Technol.*, vol. 54, no. 3, pp. 151–160, Oct. 2016.

[15] T. A. Kumar, K. Premalatha, and A. M. Natarajan, "Hand vein pattern recognition using natural image statistics," *Defence Sci. J.*, vol. 65, no. 2, pp. 150–158, Mar. 2015.

[16] K. Premalatha, A. Kumar, and A. Natarajan, "A dorsal hand vein recognition based on local Gabor phase quantization with whitening transformation," *Defence Sci. J.*, vol. 64, no. 2, pp. 159–167, Mar. 2014.

[17] Y. Wang and X. Zheng, "Cross-device hand vein recognition based on improved SIFT," *Int. J. Wavelets, Multiresolution Inf. Process.*, vol. 16, no. 02, Mar. 2018, Art. no. 1840010.

[18] R. Wang, G. Wang, Z. Chen, Z. Zeng, and Y. Wang, "A palm vein identification system based on Gabor wavelet features," *Neural Comput. Appl.*, vol. 24, no. 1, pp. 161–168, Jan. 2014.

[19] Z. Meng and X. Gu, "Hand vein identification using local Gabor ordinal measure," *J. Electron. Imag.*, vol. 23, no. 5, Sep./Oct. 2014, Art. no. 053004.

[20] H. Yun-Peng, W. Zhi-Yong, Y. Xiao-Ping, and X. Yu-Ming, "Hand vein recognition based on the connection lines of reference point and feature point," *Infr. Phys. Technol.*, vol. 62, pp. 110–114, Jan. 2014.

[21] D. Hartung, M. A. Olsen, H. Xu, H. T. Nguyen, and C. Busch, "Comprehensive analysis of spectral minutiae for vein pattern recognition," *IET Biometrics*, vol. 1, no. 1, pp. 25–36, Mar. 2012.

[22] A. Kumar and K. V. Prathyusha, "Personal authentication using hand vein triangulation and knuckle shape," *IEEE Trans. Image Process.*, vol. 18, no. 9, pp. 2127–2136, Sep. 2009.

[23] L. Wang, G. Leedham, and D. S.-Y. Cho, "Minutiae feature analysis for infrared hand vein pattern biometrics," *Pattern Recognit.*, vol. 41, no. 3, pp. 920–929, Mar. 2008.

[24] M. U. Akram, H. M. Awan, and A. A. Khan, "Dorsal hand veins based person identification," in *Proc. 4th Int. Conf. Image Process. Theory, Tools Appl. (IPTA)*, Paris, France, Oct. 2014, pp. 289–294.

[25] J. Wang, K. Yang, Z. Pan, G. Wang, M. Li, and Y. Li, "Minutiae-based weighting aggregation of deep convolutional features for vein recognition," *IEEE Access*, vol. 6, pp. 61640–61650, Oct. 2018.

[26] S.-J. Chuang, "Vein recognition based on minutiae features in the dorsal venous network of the hand," *Signal, Image Video Process.*, vol. 12, no. 3, pp. 573–581, Mar. 2018.

[27] A. Arakala, H. Hao, S. Davis, and K. J. Horadam, "The palm vein graph feature extraction and matching," in *Proc. ICISSP*, Angers, France, 2016, pp. 295–303.
[28] A. Arakala, H. Hao, S. Davis, and K. J. Horadam, "The palm vein graph for biometric authentication," in *Proc. ICISSP*, Angers, France, 2016, pp. 199–218.
[29] S. M. Lajevardi, K. J. Horadam, A. Arakala, and S. Davis, "Hand vein authentication using biometric graph matching," *IET Biometrics*, vol. 3, no. 4, pp. 302–313, Dec. 2014.
[30] D. Zhong, H. Shao, and S. Liu, "Towards application of dorsal hand vein recognition under uncontrolled environment based on biometric graph matching," *IET Biometrics*, vol. 8, no. 2, pp. 159–167, Mar. 2019.
[31] D. Zhong, H. Shao, and X. Du, "A hand-based multi-biometrics via deep hashing network and biometric graph matching," *IEEE Trans. Inf. Forensics Security*, vol. 14, no. 12, pp. 3140–3150, Dec. 2019.
[32] A. Arakala, S. A. Davis, H. Hao, and K. J. Horadam, "Value of graph topology in vascular biometrics," *IET Biometrics*, vol. 6, no. 2, pp. 117–125, Mar. 2017.
[33] K. Riesen and H. Bunke, "Approximate graph edit distance computation by means of bipartite graph matching," *Image Vis. Comput.*, vol. 27, no. 7, pp. 950–959, Jun. 2009.
[34] S. M. Lajevardi, A. Arakala, S. A. Davis, and K. J. Horadam, "Retina verification system based on biometric graph matching," *IEEE Trans. Image Process.*, vol. 22, no. 9, pp. 3625–3635, Sep. 2013.
[35] D. Zhang, Z. Guo, G. Lu, L. Zhang, Y. Liu, and W. Zuo, "Online joint palmprint and palmvein verification," *Expert Syst. Appl.*, vol. 38, no. 3, pp. 2621–2631, Mar. 2011.
[36] L. Zhang, H. Li, P. Shen, G. Zhu, J. Song, S. A. A. Shah, M. Bennamoun, and L. Zhang, "Improving semantic image segmentation with a probabilistic superpixel-based dense conditional random field," *IEEE Access*, vol. 7, p. 1, Mar. 2018.
[37] R. B. Trabelsi, A. D. Masmoudi, and D. S. Masmoudi, "Hand vein recognition system with circular difference and statistical directional patterns based on an artificial neural network," *Multimedia Tools Appl.*, vol. 75, no. 2, pp. 687–707, Jan. 2016.
[38] W. Damak, R. B. Trabelsi, M. A. Damak, and D. Sellami, "Dynamic ROI extraction method for hand vein images," *IET Comput. Vis.*, vol. 12, no. 5, pp. 586–595, Aug. 2018.

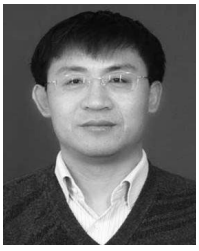

FU LIU received the B.S. and M.S. degrees from the Jilin University of Technology, in 1991 and 1994, respectively, and the Ph.D. degree from the Department of Control Science and Engineering, Jilin University, in 2002. He is currently a Professor with Jilin University. His research interests include machine vision, pattern recognition, bioinformatics, and biometrics.

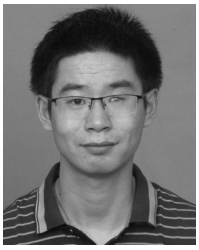

SHOUKUN JIANG received the B.S. degree from the College of Communication and Engineering, Jilin University, where he is currently pursuing the Ph.D. degree with the Laboratory of Pattern Recognition and Artificial Intelligence, College of Communication and Engineering. His research areas include machine learning and biometric recognition.

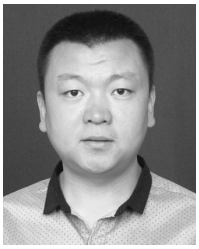

BING KANG received the B.S. degree from the College of Electrical and Electronic Engineering, Changchun University of Technology, and the M.S. degree from the College of Computer Science and Technology, Jilin University, and the Ph.D. degree from the College of Communication and Engineering, Jilin University. He is currently a Senior Engineer with Jilin University. His areas of research include machine learning and biometric recognition.

TAO HOU received the B.S. degree from the College of Mathematics, Jilin University, and the M.S. and Ph.D. degrees from the College of Communication and Engineering, Jilin University. She is currently a Lecturer with Jilin University. Her areas of research include machine learning and bioinformatics.